Overcoming Efficiency Degradation in Wireless Power Transfer Systems: A Supply Voltage Modulation Method Empowered by 5.64-GHz 256-Element Antenna Array Receiving 10.6-Watt

Taeyeong Yoon[12], Young-Seok Lee[12], Minje Kim[12], Sanghun Lee[12], Jaesup Lee[3], Sangwook Nam[12], Jungsuek Oh[12]
[1]Institute of New Media and Communications (INMC), Seoul National University, Republic of Korea
[2]Department of Electrical and Computer Engineering, Seoul National University, Republic of Korea
[3]Samsung Advanced Institute of Technology, Republic of Korea
taeyeong.yoon@snu.ac.kr, jungsuek@snu.ac.kr

2025 IEEE/MTT-S International Microwave Symposium - IMS 2025 | 979-8-3315-1409-9/25/$31.00 ©2025 IEEE | DOI: 10.1109/IMS40360.2025.11104047

***Abstract*— This paper proposes a supply voltage switching method for a 16 × 16 large-scale array system operating at 5.64 GHz to efficiently receive radio frequency power, considering transmitter hardware efficiency—a factor not extensively addressed in previous wireless power transfer (WPT) research. This study focuses on improving both transmitter efficiency (η_{tx}) and free-space efficiency (η_{air}). We optimize η_{air} by determining each element's transmission amplitude and phase through convex optimization. However, this requires amplitude tapering of approximately 50 dB or more, negatively affecting η_{tx}. To address this degradation, we propose techniques to enhance the product of the two efficiencies and conduct experiments using an implemented system. Comparing the commonly used time-reversal pattern in WPT with the proposed convex pattern, we demonstrate that the proposed method improves η_{air} from 62 % to 78 % ideally. Additionally, the measured received power was 10.6 W for 5 × 5 array configuration at 0.5 m distance.**

***Keywords*— Efficiency enhancement, time-reversal (TR), radio-frequency (RF), wireless power transfer (WPT), convex optimization, amplitude tapering.**

I. Introduction

Wireless power transfer (WPT) technology using antenna arrays has recently gained widespread adoption, offering a convenient, wire-free power supply with higher efficiency over relatively long distances compared to inductive coupling methods. This technology could be applied to various wireless devices such as smartphones and wearables [1], and research focuses on applications and performance improvements to maintain efficiency over long distances [2].

WPT systems are classified into near-field and far-field operations based on distance. In the far-field, conventional beamforming techniques apply amplitude and phase adjustments to the array; however, in the near-field, various patterns are proposed due to the difficulty in determining the efficiency. The most commonly used pattern is time-reversal (TR), constructed by conjugating the phase captured at the transmitter from a pilot signal at the desired focus location. Although straightforward to implement, TR does not provide optimal efficiency [3]. Convex (CVX) optimization using the channel matrix yields a solution with optimal efficiency and has been recently applied in near-field WPT systems [4], deriving optimal free-space and receiver efficiencies using semidefinite relaxation (SDR). As the distance increases, the solution converges to beamforming feature, making it more analogous to conventional far-field techniques. However, prior research lacks an analysis of transmitter hardware efficiency, which remains unconsidered. Interestingly, we found that the CVX-optimized pattern deteriorates transmitter efficiency due to severe amplitude tapering which is a primary factor enhancing the efficiency, with maximum and minimum values of 30 and -20,dB, respectively, as shown in Fig. 1(b); the TR pattern also exhibits moderate amplitude tapering negatively affecting transmitter efficiency, as shown in Fig. 1(a). Therefore, we propose a supply voltage switching method to mitigate this degradation and enhance efficiency, providing analysis and justification for the switching levels.

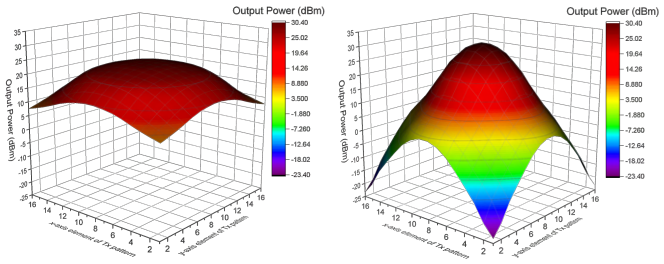

(a) (b)

Fig. 1. The 3D map displaying each transmitting element's output power distribution for (a) time-reversal and (b) convex patterns.

II. Devolopement of WPT System

Fig. 2(a) shows a typical WPT system configuration. The transmitter comprises a direct current (DC) power source—represented as a switched-mode power supply (SMPS)—a transmitter block with adjustable phase and amplitude to emit power sequences, and an antenna array of dimensions $N_t \times M_t$. The receiver includes a rectifier that converts received radio frequency (RF) power from an $N_r \times M_r$ antenna array into DC, and a DC-DC converter to adjust voltage levels required by various devices. Efficiency is classified into three types: η_{tx}, the efficiency of the transmitter hardware and wave characteristics formed by the antenna array's phase and amplitude; η_{air}, the power transfer efficiency

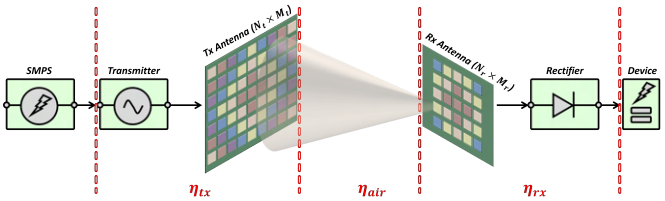

(a)

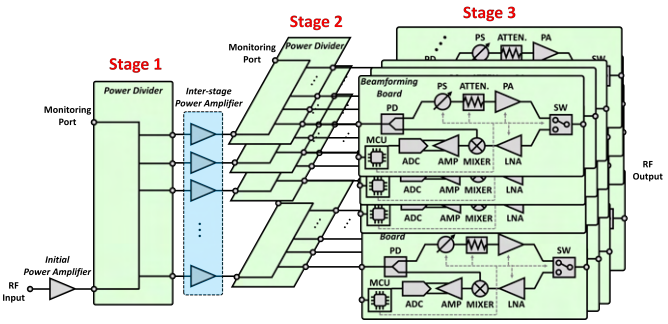

(b)

Fig. 2. (a) The schematic representing each efficiency and (b) the block diagram of the transmitter of the proposed WPT system.

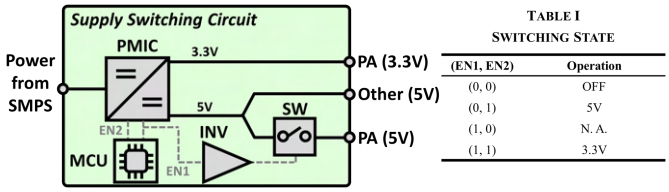

TABLE I
SWITCHING STATE

(EN1, EN2)	Operation
(0, 0)	OFF
(0, 1)	5V
(1, 0)	N. A.
(1, 1)	3.3V

Fig. 3. The schematic of the supply voltage switching circuit for the proposed system with the table for each state.

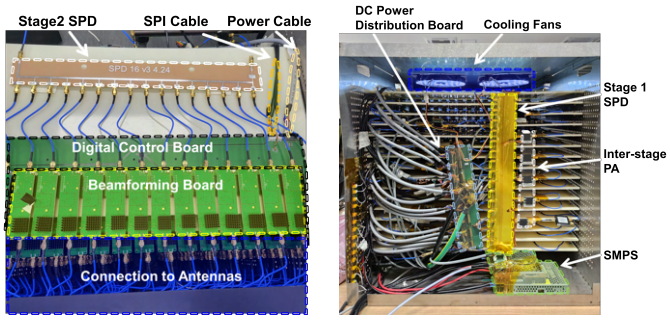

(a) (b)

Fig. 4. (a) The transmitter hardware prototype and (b) the rear view of the proposed WPT system.

through the air; and η_{rx}, the efficiency of converting received RF power into DC power.

Fig. 2(b) illustrates the proposed WPT transmitter configuration. A 16×16 array is constructed using a power divider based on sequential series power splitting theory. Monitoring ports are added to each divider to verify proper power transmission during integration and facilitate debugging [5], [6], [7]. In Stage 2, each divider equally distributes power to 16 elements within the same layer, enabling transmission to 256 elements by stacking 16 layers. Stage 1 uses a divider to split power from a single RF input into 16 equal parts, ensuring uniform power transfer across the system. Stage 3 comprises transmitting elements capable of both transmitting and receiving modes for the TR pattern. In transmitting mode, phase and amplitude are adjusted using a 4-bit phase shifter and a 7-bit attenuator on the beamforming board. Due to limitations in controlling every board with a single field-programmable gate array (FPGA), a cascading topology of microcontroller units (MCUs) is employed for each element and stage; the serial peripheral interface (SPI) facilitates communication between MCUs and the board. Finally, the transmitter's master MCU is controlled via universal asynchronous receiver/transmitter (UART) communication from a personal computer (PC).

It should be noticed that, although TR and CVX methods have been applied to enhance η_{air}, there is insufficient analysis of the hardware efficiency (η_{tx}) affected during amplitude adjustment. To address this, we propose a supply voltage switching circuit, as shown in Fig. 3; the problem is discussed in the following subsection, which analyzes efficiency measurements of the fabricated beamforming board's elements. Since the power amplifier (PA) requires a supply voltage ranging from 3.3 V to 5 V for typical operation (per the datasheet), we implemented a switchable dual supply voltage using a dual-channel DC-DC converter as a power management integrated circuit (PMIC); each PMIC channel is controlled by enable pins (EN1 and EN2 in Fig. 3). To prevent short circuits between the 3.3 V and 5 V supply paths for the PA, a switch is incorporated in the 5 V path, controlled by $\overline{\text{EN1}}$, the complement of EN1 obtained via an inverter. Under normal conditions (EN1=0 and EN2=1), the circuit supplies 5 V to the PA and other circuits. When EN1=1 and EN2=1, the PA operates at 3.3 V—offering higher efficiency but lower saturation output power—while maintaining a 5 V supply for other circuits. A turn-off state is achieved when EN1=0 and EN2=0, saving redundant power consumption (i.e., the PA's quiescent current) when transmitting low output powers for TR and CVX patterns. The supply voltage changes corresponding to the enable pin states are summarized in Table I.

Hardware integration is depicted in Fig. 4(a) and (b). Stage 2 consists of 16 layers, each connected to 16 beamforming boards interfacing with the antenna array. Each layer includes a digital control board featuring an MCU that controls all 16 elements via SPI communication and manages power delivery. The beamforming boards, shown in Fig. 4(a), are secured using connection pins and a nylon jig. A heat sink attached to the thermal paste dissipates heat generated by the PA.

A DC power distribution board, powered by the SMPS, supplies power to all 16 layers and is mounted on the rear of the transmitter, as shown in Fig. 4(b). This figure also illustrates connections between the Stage 1 power divider and inter-stage PAs. The board includes a heat sink to address heat dissipation, and the case is constructed from metal. Cooling fans powered by the DC power distribution board are installed

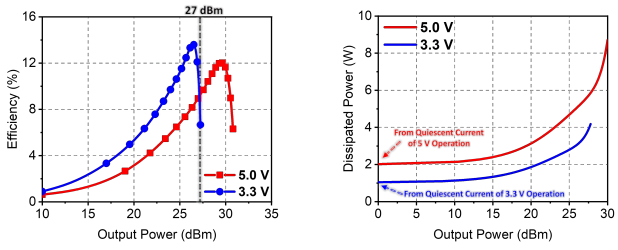

(a) (b)

Fig. 5. The measured results of (a) efficiency and (b) dissipated power of the beamforming board for each supply voltage at 5.64 GHz.

on the top and sides to facilitate heat removal.

Proper phase and amplitude adjustment using methods like TR and CVX patterns is essential to efficiently transmit power through the air (η_{air}). However, adjusting amplitude via the attenuator controls the PA's output power but degrades transmitter hardware efficiency (η_{tx}) because the PA's efficiency varies with output power levels. While many studies focus on enhancing η_{air}, this paper addresses the hardware efficiency degradation caused by amplitude control and proposes a solution. We evaluated the transmitter hardware efficiency of the proposed WPT system using TR and CVX patterns by measuring efficiency and power consumption relative to the beamforming board's output power at 5.64 GHz, as shown in Fig. 5. Output power was adjusted using the onboard attenuator, and measurements were taken by switching the supply voltage between 3.3 V and 5 V using the circuit in Fig. 3. Results show saturation output powers of 28 dBm for 3.3 V and 31 dBm for 5 V. Notably, 3.3 V operation is more efficient up to 27 dBm output power, while 5 V is more efficient above 27 dBm. Thus, both voltage operations should be utilized appropriately.

Two key observations are: (1) Peak efficiencies for 3.3 V and 5 V occur at different output power levels, suggesting efficiency can be improved during amplitude tapering by switching supply voltage; (2) Efficiency drops significantly for both voltages as output power approaches lower value as illustrated in Fig. 5(a). This is due to the PA's quiescent current causing constant power consumption (2 W at 5 V, 1 W at 3.3 V) even at low output powers, as shown in Fig. 5(b). In WPT systems utilizing the CVX pattern for efficiency improvement, amplitude tapering can vary power levels by over 50 dB, where meager output powers contribute little to radiation performance but cause unnecessary power consumption. To address this, the following subsection analyzes the threshold where output power becomes inefficient within the pattern's power range.

As shown in Fig. 1(a) and (b), the output power distributions for both TR and CVX patterns have distinct maximum and minimum values. While these specific output levels are expected to have minimal impact on overall free-space efficiency, the turn-off state at certain threshold levels could degrade free-space efficiency. However, this may enhance transmitter hardware efficiency. To balance these

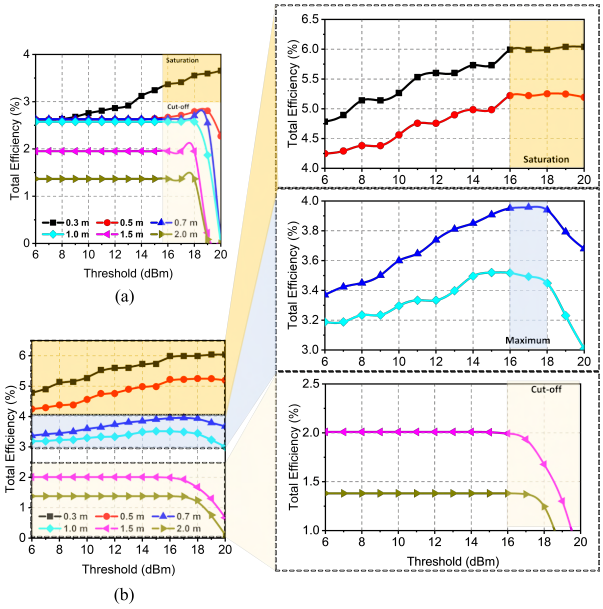

Fig. 6. The total efficiency of (a) time-reversal and (b) convex with respect to different threshold power and distance.

opposing tendencies, we define the total efficiency as the product of the two efficiencies, as expressed in (1), and propose a method to optimize this combined efficiency.

$$\eta_{total}(\%) = \eta_{tx} \times \eta_{air} \tag{1}$$

$$\begin{cases} 5\,\text{V}, & P_{out} > 27\,\text{dBm} \\ 3.3\,\text{V}, & 16\,\text{dBm} < P_{out} < 27\,\text{dBm} \\ \text{Turn-off}, & P_{out} < 16\,\text{dBm} \end{cases} \tag{2}$$

Ultimately, the CVX pattern enables determining the optimal threshold power due to the opposing tendencies of η_{tx} and η_{air}. The opposing behaviors of the two efficiencies result in a saturation effect on total efficiency. The results for TR and CVX patterns at various distances under identical conditions are also presented in Fig. 6(a) and (b). Comprehensive analysis reveals that the threshold power corresponding to saturation, maximum efficiency, and cut-off consistently occurs around 16 dBm. Based on this observation, we set the threshold power for the turn-off state in the proposed WPT system at 16 dBm. The superiority of our study can be understood through (3), which compares the power consumption and efficiency required to transmit 20 W between the conventional method using only 5 V and the proposed method that appropriately utilizes 5 V, 3.3 V, and the turn-off state as a supply voltage. Specifically focusing on the CVX results, the power consumption decreased from 725 W to 237 W, achieving an improved total efficiency of 5.95 %. Additionally, the measured RF power results from the setup in Fig. 7(a) confirm that under ideal channel modeling conditions, as shown in Fig. 7(b), a total of 12.5 W was received by the 5 $\times$ 5 receiver array. The top and bottom layers were

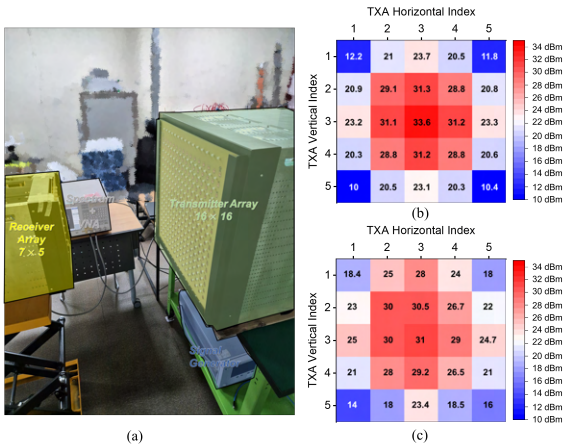

Fig. 7. (a) The measurement environment and the results of the received RF power for (b) ideal condition and (c) measurement at 0.5 m distance.

Table 2. Comparison with recently published papers

Ref.	# of Tx Elements	Received Power (W)	η_{air} (%)	η_{tx} (%)	Distance (λ)
[8]	9	0.37	3.2	24*	8
[9]	64	0.16	0.5	–	69
[10]	16	0.007	0.54	–	77
[11]	16	0.5	12.5	–	4
This work	256	10.6	59.2	8	9.4

* Since the transmitting pattern does not involve amplitude tapering, the value is directly inferred from the efficiency of the PA.

implemented as dummy elements to ensure a stable radiation pattern. The measured results, depicted in Fig. 7(c), indicate that 10.6 W was received while forming a similar pattern to the ideal pattern. Table II compares the performance of the proposed WPT system with that of recently published works. To account for the effect of frequency on distance, the distance is expressed in terms of its ratio to the free-space wavelength. Furthermore, by incorporating an analysis of η_{tx}, we provide a more comprehensive perspective on efficiency and demonstrate improvements in areas where performance had previously degraded.

$$\begin{cases} P_{diss} = 725W \,\&\, \eta_{total} = 2.75\%, & \text{Conventional (CVX)} \\ P_{diss} = 237W \,\&\, \eta_{total} = 5.95\%, & \text{Proposed (CVX)} \end{cases} \tag{3}$$

III. Conclusion

This paper proposed a voltage switching method to enhance η_{tx} in WPT systems, which has not been extensively addressed until now. While many studies employ amplitude tapering methods to improve η_{air}, these methods reduce η_{tx}. To compensate for this degradation, we present an analysis of the threshold for appropriate switching with three states. The proposed method was validated using a transmitter with a 16 $\times$ 16 array and a receiver with a 5 $\times$ 5 array. As a result, we confirmed that 17.9 W was transmitted while consuming 237 W of power, and 10.6 W was received at a distance of 0.5 m.

Acknowledgment

This research is supported in part by the A-Laboratory, Samsung Electronics (50%) and in part by Institute of Information & communications Technology Planning & Evaluation (IITP) Grant funded by the Korea Government[Ministry of Science and ICT (MSIT)], Innovative Fusion Technologies of Intelligent Antenna Material/Structure/Network for THz 6G (50%), under Grant 2021-0-00763.

References

[1] H. Jung and B. Lee, "Wireless power and bidirectional data transfer system for iot and mobile devices," *IEEE Trans. Ind. Electron.*, vol. 69, no. 11, pp. 11 832–11 836, 2021.

[2] J. H. Park, D. I. Kim, and K. W. Choi, "Analysis and experiment on multi-antenna-to-multi-antenna rf wireless power transfer," *IEEE Access*, vol. 9, pp. 2018–2031, 2020.

[3] Z.-Q. Luo, W.-K. Ma, A. M.-C. So, Y. Ye, and S. Zhang, "Semidefinite relaxation of quadratic optimization problems," *IEEE Signal Process. Mag.*, vol. 27, no. 3, pp. 20–34, 2010.

[4] S. Shen and B. Clerckx, "Beamforming optimization for mimo wireless power transfer with nonlinear energy harvesting: Rf combining versus dc combining," *IEEE Trans. Wirel. Commun.*, vol. 20, no. 1, pp. 199–213, 2020.

[5] V. Rafii, J. Nourinia, C. Ghobadi, J. Pourahmadazar, and B. S. Virdee, "Broadband circularly polarized slot antenna array using sequentially rotated technique for *c*-band applications," *IEEE Antennas Wireless Propag. Lett.*, vol. 12, pp. 128–131, 2013.

[6] Y.-S. Lee, T. Yoon, M. Kim, S. Lee, B. Jung, J. Oh, and S. Nam, "A design and characterization method of a scalable large transmitting array for wireless power transfer," *IEEE Trans. Microw. Theory Tech.*, 2024.

[7] Y.-S. Lee, T. Yoon, S. Lee, M. Kim, J. Lee, J. Oh, and S. Nam, "Lut-based transmit mode calibration complexity reduction method for wireless power transfer," in *2024 IEEE Wireless Power Technology Conference and Expo (WPTCE)*. IEEE, 2024, pp. 137–141.

[8] L. Hu, X. Ma, G. Yang, Q. Zhang, D. Zhao, W. Cao, and B.-Z. Wang, "Auto-tracking time reversal wireless power transfer system with a low-profile planar rf-channel cascaded transmitter," *IEEE Trans. Ind. Electron.*, vol. 70, no. 4, pp. 4245–4255, 2022.

[9] H. Koo, J. Bae, W. Choi, H. Oh, H. Lim, J. Lee, C. Song, K. Lee, K. Hwang, and Y. Yang, "Retroreflective transceiver array using a novel calibration method based on optimum phase searching," *IEEE Trans. Ind. Electron.*, vol. 68, no. 3, pp. 2510–2520, 2020.

[10] D. Belo, D. C. Ribeiro, P. Pinho, and N. B. Carvalho, "A selective, tracking, and power adaptive far-field wireless power transfer system," *IEEE Trans. Microw. Theory Tech.*, vol. 67, no. 9, pp. 3856–3866, 2019.

[11] P. D. H. Re, S. K. Podilchak, S. A. Rotenberg, G. Goussetis, and J. Lee, "Circularly polarized retrodirective antenna array for wireless power transmission," *IEEE Trans. Antennas Propag.*, vol. 68, no. 4, pp. 2743–2752, 2019.